Direct electrochemical formation of alloyed AuPt nanostructured electrocatalysts for the oxidation of formic acid

Ali Balkis and Anthony P. O'Mullane*

School of Applied Sciences, RMIT University, GPO Box 2476V, Melbourne, VIC 3001, Australia

Email: anthony.omullane@rmit.edu.au

Keywords: alloys, nanostructures, electrochemical techniques, electrochemical properties

Abstract

The formation of highly anisotropic AuPt alloys has been achieved via a simple electrochemical approach without the need for organic surfactants to direct the growth process. The surface and bulk properties of these materials were characterised by scanning electron microscopy (SEM), X-ray diffraction (XRD), energy dispersive X-ray spectroscopy (EDX) and electrochemically by cyclic voltammetry to confirm alloy formation. It was found that AuPt materials are highly active for both the model hydrogen evolution reaction and the fuel cell relevant formic acid oxidation reaction. In particular for the latter case the preferred dehydrogenation pathway was observed at AuPt compared to nanostructured Pt prepared under identical electrochemical conditions which demonstrated the less preferred dehydration pathway. The enhanced performance is attributed to both the ensemble effect which facilitates $CO_{(ads)}$ removal from the surface as well as the highly anisotropic nanostructure of AuPt.

1. Introduction

The electrochemical formation of metallic nanostructured materials is a burgeoning area of research interest. This is due to the high level of compositional, shape and size control that is achievable using electrochemical methods under ambient conditions [1-6]. There is a significant amount of literature on the electrodeposition of metallic nanostructures based on gold [7-9], platinum [10-12], palladium [13-15], silver [4, 16-17] and copper [18-20] where the influence of size, shape and exposed crystal facets play key roles in electrocatalytic performance [21]. Indeed this approach offers a highly beneficial means to study the electrocatalytic performance of such materials without the complication of organic capping agents that are typically used in the chemical synthesis of nanomaterials to prevent aggregation.

In electrocatalysis the oxidation of small organic molecules in particular has received attention in relation to fuel cell technology [22]. Methanol, ethanol, formaldehyde and also formic acid have been identified as alternative fuels to hydrogen for commercially applicable fuel cells. Although the energy density of formic acid is less than that of methanol it generally has less problems associated with crossover through the electrolyte membrane which therefore in principle would allow a fuel cell to operate with higher fuel concentrations and thinner membranes [23]. The oxidation of formic acid is known to proceed via a dual path mechanism on platinum, i.e. a preferred dehydrogenation pathway which is direct oxidation to CO_2 and the less preferred dehydration pathway where $CO_{(ads)}$ is generated as an intermediate which poisons the electrocatalyst surface [23-24]. Many strategies have been employed to promote the direct pathway, however a particularly successful approach is using a bimetallic electrocatalyst based on platinum where the secondary metal is typically Au or Pd [23, 25-29]. An added advantage of bimetallic systems is that electrodissolution of the electrocatalyst can be minimised [30].

However, in comparison to chemically synthesised bimetallic nanoparticles there have been comparatively fewer studies on the direct electrodeposition of bimetallic nanostructured materials. The advantage of employing bimetallic materials are well known in the areas of catalysis and electrocatalysis, due to the synergistic effect often seen when metals are combined over their individual components. As mentioned previously the AuPt and PtPd combination influences the formic acid oxidation reaction mechanism. Often the synergistic effect is as a result of electronic perturbation effects which influences the adsorption of reactants and intermediates and desorption of products from the surface that can dictate the rate of reaction. Recently Greely et al have shown by density functional theory calculations the influence of a vast array of bimetallic combinations on the metal – hydrogen bond strength which plays a key role in the hydrogen evolution reaction [31-32]. A key aspect to enhanced formic acid oxidation is the fabrication of an alloyed rather than phase separated material in particular for AuPt [23, 25, 27]. Due to the miscibility gap between Pt and Au in their binary phase diagram the synthesis of an alloyed material is often challenging [27]. The chemical synthesis of nanostructured AuPt alloys can be quite involved and usually requires organic surfactants and/or elevated temperatures and prolonged reaction times. Therefore the ability to rapidly produce AuPt alloys in the absence of organic moieties would be particularly useful for electrocatalytic applications.

In this work the direct electrodeposition of AuPt nanostructures is reported in the absence of any surfactants from a simple electroplating bath containing equimolar concentration of an aqueous solution containing $HAuCl_4$ and K_2PtCl_4. The morphology and composition is dependent on the applied deposition potential and significantly it is shown that an alloy is formed which is particularly beneficial for the direct oxidation of formic acid.

2. Experimental

Chemicals: Aqueous solutions of $HAuCl_4$, K_2PtCl_4 (Aldrich), formic acid (Merck), H_2SO_4, HCl (Ajax Finechem) were made up with deionised water (resistivity 18.2 MΩ) purified by use of a Milli-Q reagent deioniser (Millipore). Pt/C – 20 wt % Pt on carbon (Alfa Aesar) was used as a commercial catalyst.

Electrochemical measurements: Cyclic voltammetric experiments were conducted (22 ± 2) °C with a CH Instruments (CHI 760C) electrochemical analyser in an electrochemical cell (BAS) that allowed reproducible positioning of the working, reference, and counter electrodes and a nitrogen inlet tube. The GC electrodes (0.126 cm^2 – GC plates (1 x 0.75 x 0.3 cm) were masked off using Kapton tape) were polished on a polishing cloth (Microcloth, Buehler), and rinsed with Milli-Q water, sonicated in acetone for 5 minutes and then ethanol for a further 5 minutes, and dried with nitrogen gas. The reference electrode was Ag/AgCl (aqueous 3M KCl). For all of the electrochemical experiments carried out, an inert graphite rod (5 mm diameter, Johnson Matthey Ultra "F" purity grade) was used as the counter electrode to prevent contamination by any possible electrolysis products during electrodeposition [33]. To investigate the commercial Pt/C catalyst a total of 5 mg of the catalyst was mixed with 0.12 mL of 5 wt % Nafion in 3.88 mL of ethanol to obtain a suspension. 5 μL of this solution was drop cast onto the GC plate and allowed to dry. All electrochemical experiments were commenced after degassing the electrolyte solutions with nitrogen for at least 10 min prior to any measurement.

Instrumentation: SEM measurements were performed on a FEI Nova SEM instrument with an AMETEK energy dispersive X-ray (EDX) system (Nova 200) operated at an accelerating voltage of 30 kV. Prior to SEM imaging, samples were thoroughly rinsed with Milli-Q water and dried under a flow of nitrogen. X-Ray diffraction (XRD) measurements were conducted on a Bruker AXS X-ray diffraction system with an operating voltage and current of 40 kV and

40 mA with CuKα radiation. XPS was performed using a Thermo K-Alpha instrument at a pressure better than 10^{-9} Torr, with the data being referenced to the adventitious C 1s binding energy of 285 eV.

The following table describes the experimental conditions employed to create the samples used in this study. In all cases the electrodeposition time was held constant at 600 s.

Sample no.	Electrodeposition potential [V] vs Ag/AgCl	Electrolyte Supporting electrolyte of 0.1 M HCl was used in all cases
S1	-0.20	2.5 mM K_2PtCl_4
S2	-0.20	2.5 mM $HAuCl_4$
S3	0.25	2.5 mM $HAuCl_4$ + 2.5 mM K_2PtCl_4
S4	0.00	2.5 mM $HAuCl_4$ + 2.5 mM K_2PtCl_4
S5	-0.20	2.5 mM $HAuCl_4$ + 2.5 mM K_2PtCl_4

Table 1: Experimental parameters used in the preparation of electrodeposited samples.

3. Results and discussion

Illustrated in Figure 1 are cyclic voltammograms (CVs) for the electrodeposition of Au, Pt and AuPt on to a GC electrode from electrolytes containing 2.5 mM K_2PtCl_4, 2.5 mM $HAuCl_4$ and an equimolar (2.5 mM) solution of both salts in a supporting electrolyte of 0.1 M HCl respectively. The latter was added to maintain the solubility of the salts in the mixed solution as in its absence a minor brown precipitate was formed presumably due to $Au(OH)_{3(s)}$ [34]. The CVs demonstrate that the electrodeposition of Au is more facile on GC than Pt due to the large difference in the onset potential which occurs at 0.50 V and -0.02 V for Au and Pt respectively. In both cases on the reverse sweep a current cross over is observed which is indicative of a nucleation-growth process [35-36]. It should be noted that the slightly greater

increase in current seen at the end of the sweep in the case of Pt electrodeposition is due to the hydrogen evolution reaction (HER). The CV recorded at GC of the mixed salt solution shows two distinct processes, a shoulder at ca. 0.20 V and a broad response from 0.20 V until the end of the reduction sweep. The onset potential occurs at 0.35 V which is less positive than in the case of $HAuCl_4$ only (Figure 1b). This suggests that the response recorded is not simply a superimposition of the two individual processes and that there may be some speciation changes which makes metal electrodeposition on GC more difficult. It appears that the gold electrodeposition process is shifted negatively and the Pt deposition process positively. The latter is expected as the overpotential for Pt deposition on Au is assumed to be less than that on bare GC. This type of effect has been seen previously for the electrodeposition of CuPd alloys from ionic liquid electrolytes [37].

The effect of the applied potential was investigated as this can offer control over morphology, as seen by various studies of the electrodeposition of single metallic structures [2, 7-8] and composition when co-depositing two metals [37-40]. The relevant electrodeposition parameters are shown in Table 1. Initially the same conditions were employed for the deposition of Pt, Au and AuPt, i.e. an applied potential of -0.20 V for 600 s. In the case of Pt deposition only (S1) the surface consists of quasi spherical particles with sizes grouped into distinct size regimes of 100 and 400 nm diameter which consist of agglomerated smaller nanoparticles (Figure 2a). For the electrodeposition of Au only (S2) the coverage is significantly greater (Figure 2b) as expected due to the more facile reduction of Au on GC compared to Pt (Figure 1). The surface consists of a relatively monodisperse coverage of gold nanoparticles of ca. 150 nm in diameter. Illustrated in Figure 3a are SEM images of nanostructures electrodeposited from the mixed salt solution where it can be seen that surface coverage, size and shape of the nanostructures are distinctly different. The surface coverage lies between that observed for the Au and Pt only cases. The size of the

nanostructures is in the range of 300 – 500 nm which are evenly dispersed over the GC substrate. Therefore it appears that the AuPt nanostructures size is closer to that observed in the case of Pt only deposition. However, it is the morphology of the deposit which shows the greatest difference from that observed for the individual Au and Pt nanomaterials. The nanostructures are no longer quasi spherical in nature but highly anisotropic with a fractal or dendritic type structure. They appear to be truncated dendrites as there is no evidence of an elongated backbone structure which is observed for many electrodeposited metals. The evolution of this type of nanostructure can be seen from the effect of the applied potential. At a more positive deposition potential of 0.00 V (S4) the nanostructures are still anisotropic but possess fewer sharp protrusions and are more block like in nature. Increasing the deposition potential to 0.25 V (S3) the deposit resumes its quasi spherical nature but the surface is quite rough with numerous block like crystallites which are assumed to be the nucleation points for the anisotropic growth of AuPt at the more negative potentials.

Under these conditions given that Au will be deposited before Pt it appears that the co-deposition of Pt with Au perturbs the Au crystal growth process which results in anisotropic nanostructures. The applied potential alone does not result in perturbation of the nanostructure as Au electrodeposited at 0.25, 0.00 and -0.20 V did not show any morphology change (Figure S1). The only difference that was observed was the surface coverage which is expected to increase on decreasing the potential. Therefore the competing Pt and Au deposition processes results in growth in preferred directions which is beneficial as often in chemical synthesis the use of surfactants is required to promote dendritic type growth, as seen for Au core / Pt shell materials where pluronic surfactants were required for the formation of an outer dendritic Pt shell [41]. However, a recent report demonstrated that AuPt and PtPb nanodendrites could be produced hydrothermally using formic acid as a reductant at a temperature of 180°C for 8 hr [42]. Again the advantage of an electrochemical route is

evident here by the rapid synthesis time of 10 min at room temperature. It has been reported that dendritic type growth can be regarded as a competition between the order associated with crystal symmetry, as is the case for the deposition of Pt and Au only, and instabilities that are induced in the system such as non linear diffusion [42] or the presence of foreign species. In the case of AuPt formation the latter would be the dominant factor as the crystal growth of Au is perturbed by the presence of Pt being incorporated into the structure. For the co-crystallisation of metals the presence of pinning centres which are considered to be the metal at the lower concentration induces disorder and results in the growth of side branches [42]. Therefore it appears that as the potential is lowered the extent of Pt deposition is expected to increase thereby increasing the density of pinning centres which results in a layered type structure with extensive branch formation and sharp protrusions which is seen to gradually evolve when comparing the high magnification SEM images of S4 and S5 in Figure 4.

The presence of Au and Pt in samples S3, S4 and S5 was confirmed by cyclic voltametric experiments in 1 M H_2SO_4 which are illustrated in Figure 5. Over the potential range of -0.25 to 0.10 V there is a clear hydrogen adsorption/desorption region which is typically associated with Pt and increases in magnitude as the electrodeposition potential is made more negative. There is a distinct cathodic peak at ca. 0.96V for samples S3, S4 and S5 which is due to the reduction of gold oxide formed on the forward sweep which also increases in magnitude due to the greater amount of material formed at lower deposition potentials. For samples S4 and S5 a peak at ca. 0.42 V is observed due to the reduction of Pt oxide formed in the forward sweep. Therefore for all samples there is clear electrochemical evidence that Au and Pt are co-deposited. The presence of both metallic Pt and Au was confirmed by EDX analysis for samples S3, S4 and S5 and is shown in Figure S2. The bulk concentrations of Pt:Au were found to be 16:84, 37:63 and 33:67 for samples S3, S4 and S5 respectively. The presence of Pt in sample S3 however was further confirmed by XPS analysis and is shown in

Figure S3 which gave characteristic peaks corresponding to metallic Pt at binding energies of 71.5 and 74.8 eV for Pt $4f_{7/2}$ and Pt $4f_{5/2}$ respectively [25].

It has been observed for bimetallic systems that the oxide reduction peak potentials of the individual components can be slightly shifted [43-44]. In Figure 5b the CVs of Pt (sample S1) and AuPt (sample S4) are compared which shows that the Pt oxide reduction peak is shifted by ca. 30 mV in the positive direction for the AuPt sample. This is also the case for sample S5 as evident from Figure 5a. It can also be seen that there is a shift in the Au oxide reduction peak to less positive potentials as Pt is incorporated into the sample which is particularly evident in sample S4 (Figure 5a). This type of shift in oxide reduction potentials is a strong indicator of AuPt alloy formation. This was confirmed by XRD experiments (Figure 6) which show the peak positions for Au (111), (200) and (220) (JCPDS 04-0784), Pt (111), (200) and (220) (JCPDS 04-0802) and the electrochemically deposited AuPt samples. For samples S4 and S5 there is a clear shift in peak positions for the (111), (200) and (220) reflections to values between those for pure Pt and pure Au and indicates the formation of a bulk single phase alloy rather than a phase separated or core-shell type material. The peak positions lie closer to that of pure Au which is not unexpected given the higher bulk concentration of Au measured by EDX experiments. For sample S3 there is no clear shift in the peak position from that of pure gold and suggests that this sample consists predominantly of gold which is supported by the EDX and CV data which showed only a minor contribution from Pt in the form of the hydrogen adsorption/desorption profile from -0.25 to 0.10 V (Figure 5a). However the possibility of some alloy formation cannot be completely ruled out. It should be noted that the peaks that are labelled with an asterisk in Figure 6 are due to the underlying GC electrode.

To test the electrocatalytic activity of these materials two reactions were studied, namely, the hydrogen evolution reaction (HER) and the oxidation of formic acid. It should be

noted that all electrocatalytic responses have been normalised for the electrochemically active surface area of Pt which was determined by the charge associated with hydrogen adsorption on Pt [45] using a value of 210 μC cm^{-2}. For AuPt it can be seen that enhanced performance was seen in all cases for the HER (Figure 7a). This is evidenced by the shift in onset potential to less positive values when compared to pure Pt and the increase in current density which are indicative of an electrocatalytic effect. Therefore the incorporation of gold has a positive influence on the specific activity of the material for the HER. Given that Au is a poorer electrocatalyst than Pt for this reaction due to the much weaker metal-hydrogen bond strength for Au compared to Pt suggests also that a phase separated material has not been formed which would be expected to decrease overall activity. In Greeley's extensive density functional theory calculations on the free energy of hydrogen adsorption (ΔG_H) on a variety of alloys showed that low solute coverages of Au in Pt had comparable ΔG_H values to pure Pt [31-32]. Therefore the increase in current density seen for the HER is most likely attributed to a morphology difference where it has been shown that anisotropic shaped materials are better electrocatalysts than smooth materials [9, 13, 46] like that seen in this case for pure Pt (Figure 1). This can be attributed to a higher density of active sites being present on the tips and sharp edges of these materials [7, 47]. Interestingly the specific activity of sample S3 for the HER was the highest (even though it should be noted that the absolute current was significantly lower for this sample compared to S4 and S5 due to the lower surface area) and therefore indicates that the Pt that is present is highly active for this particular reaction. However it should also be considered that active gold sites may be a contributing factor to this reaction.

The oxidation of formic acid was also investigated at all samples and found to be enhanced at AuPt compared to pure Pt (Figure 7b) for samples S4 and S5 only where it is clear that the measured current density is significantly greater at the AuPt alloy materials. In the case of Pt (S1), two distinct oxidation processes occur at ca. 0.36 and 0.69 V which are

related to the preferred dehydrogenation pathway that results in direct oxidation to CO_2 and the less preferred dehydration pathway where $CO_{(ads)}$ is generated as an intermediate respectively. Given the relative intensities of these peaks suggests that the reaction proceeds to a greater degree via the dehydration pathway. This is also the case for commercial Pt/C (20 wt % Pt on carbon) which shows better specific activity compared to the electrodeposited Pt but still demonstrates a significant process at higher potential due to the dehydration pathway. In the case of AuPt (S4 and S5) a prominent peak is observed at 0.42 V indicating that the direct oxidation of formic acid via the dehydrogenation pathway is favoured. Sample S3 showed significantly less activity compared to pure Pt and can be attributed to the predominance of gold in the sample which is completely inactive towards the formic acid oxidation reaction. This also demonstrates that the composition of the catalyst needs to be controlled for the specific reaction of interest given the high performance of this material for the HER. It can also be seen that the performance of sample S4 is slightly greater than that for S5. In the latter case a slight shoulder is observed at 0.73 V attributed to the dehydration pathway and therefore surface poisoning is occurring which is completely absent in the case of sample S4. These data explain why the magnitude of the response is greater at AuPt than Pt as the extent of surface poisoning by $CO_{(ads)}$ is alleviated by the presence of Au. This is due to an ensemble effect in which the dehydration reaction pathway requires at least two ensemble Pt sites, whereas the dehydrogenation reaction pathway occurs preferentially on isolated Pt atoms which would occur on a well dispersed sample [23, 25]. The change in sample morphology from spherical particles to anisotropic shaped structures as seen in samples S4 and S5 is also expected to play some role in the electrocatalytic activity for formic acid oxidation, but it is more so the change in reaction mechanism that appears to dominate the overall performance.

4. Conclusions

It has been demonstrated that AuPt alloys can be successfully electrodeposited from a plating bath consisting of $HAuCl_4$ and K_2PtCl_4 at equimolar concentration. The morphology of the deposit is controlled by the applied potential which influences the rate of deposition of both metallic Au and Pt. The preferred deposition of Au is perturbed by the inclusion of K_2PtCl_4 which competes with the Au deposition process creating pinning centres on the growing deposit which results in fractal or dendritic like bimetallic growth. The formation of an alloy material that is richer in gold content was confirmed by XRD data. The AuPt alloy showed enhanced electrocatalytic activity for both the HER and industrially important formic acid oxidation reaction. In the latter case the AuPt material exhibited the preferred dehydrogenation pathway over nanostructured Pt and the overall improved performance can be attributed to the formation of an alloy promoting the ensemble effect and the creation of a highly anisotropic nanostructure.

Acknowledgements

AOM acknowledges the ARC for a Future Fellowship (FT110100760). The authors acknowledge the facilities, and the scientific and technical assistance, of the Australian Microscopy and Microanalysis Research Facility at the RMIT Microscopy & Microanalysis Facility.

List of references

[1] L.P. Bicelli, B. Bozzini, C. Mele, L. D'Urzo, Int. J. Electrochem. Sci., 4 (2008) 356-527.

[2] B.J. Plowman, S.K. Bhargava, A.P. O'Mullane, Analyst, 136 (2011) 5107-5119.

[3] Y.-X. Chen, S.-P. Chen, Z.-Y. Zhou, N. Tian, Y.-X. Jiang, S.-G. Sun, Y. Ding, Z.L. Wang, J. Am. Chem. Soc., 131 (2009) 10860-10862.

[4] X. Qin, H. Wang, X. Wang, Z. Miao, Y. Fang, Q. Chen, X. Shao, Electrochim. Acta, 56 (2011) 3170-3174.
[5] F. Endres, D. MacFarlane, A. Abbott, Electrodeposition from Ionic Liquids, Wiley - VCH, Weinheim, 2008.
[6] L.B. Venarusso, R.H. Sato, P.A. Fiorito, G. Maia, J. Phys. Chem. C, 117 (2013) 7540-7551.
[7] B.J. Plowman, A.P. O'Mullane, S.K. Bhargava, Faraday Discussions, 152 (2011) 43-62.
[8] T.-H. Lin, C.-W. Lin, H.-H. Liu, J.-T. Sheu, W.-H. Hung, Chem. Commun., 47 (2011) 2044-2046.
[9] W. Ye, J. Yan, Q. Ye, F. Zhou, J. Phys. Chem. C, 114 (2010) 15617-15624.
[10] L. Hyun-Ju, U.H. Lee, P. Jin-Young, Y. Sang-Hoon, P. Sungho, K. Young-Uk, Chem. Asian J., 4 (2009) 1284-1288.
[11] F. Ye, J. Li, T. Wang, Y. Liu, H. Wei, J. Li, X. Wang, J. Phys. Chem. C, 112 (2008) 12894-12898.
[12] D. Yang, S. Sun, H. Meng, J.-P. Dodelet, E. Sacher, Chem. Mater. , 20 (2008) 4677-4681.
[13] G.-M. Yang, X. Chen, J. Li, Z. Guo, J.-H. Liu, X.-J. Huang, Electrochim. Acta, 56 (2011) 6771-6778.
[14] B.-K. Kim, D. Seo, J.Y. Lee, H. Song, J. Kwak, Electrochem. Commun., 12 (2010) 1442-1445.
[15] F. Jia, K.-w. Wong, R. Du, Electrochem. Commun., 11 (2009) 519-521.
[16] D.K. Sharma, A. Ott, A.P. O'Mullane, S.K. Bhargava, Coll. Surf. A, 386 (2011) 98-106.
[17] S. Cherevko, X. Xing, C.-H. Chung, Electrochem. Commun., 12 (2010) 467-470.
[18] A. Keilbach, J. Moses, R. Köhn, M. Döblinger, T. Bein, Chem. Mater., 22 (2010) 5430-5436.
[19] N.D. Nikolic, G. Brankovic, M.G. Pavlovic, K.I. Popov, J. Electroanal. Chem., 621 (2008) 13-21.
[20] J.-H. Kim, R.-H. Kim, H.-S. Kwon, Electrochem. Commun. , 10 (2008) 1148-1151.
[21] J. Solla-Gullon, F.J. Vidal-Iglesias, J.M. Feliu, Annual Reports Section "C" (Physical Chemistry), 107 (2011) 263-297.
[22] A. Rabis, P. Rodriguez, T.J. Schmidt, ACS Catalysis, 2 (2012) 864-890.
[23] Y. Kim, H.J. Kim, Y.S. Kim, S.M. Choi, M.H. Seo, W.B. Kim, J. Phys. Chem. C, 116 (2012) 18093-18100.
[24] S. Garbarino, L.D. Burke, Int. J. Electrochem. Sci., 5 (2010) 828-851.

[25] J. Liu, L. Cao, W. Huang, Z. Li, ACS Appl. Mater. Interf., 3 (2011) 3552-3558.
[26] M.D. Obradovic, A.V. Tripkovic, S.L. Gojkovic, Electrochim. Acta, 55 (2009) 204-209.
[27] J. Wang, D.F. Thomas, A. Chen, Chem. Commun., (2008) 5010-5012.
[28] F.J. Vidal-Iglesias, J. Solla-Gullón, E. Herrero, A. Aldaz, J.M. Feliu, Angew. Chem. Int. Ed., 49 (2010) 6998-7001.
[29] H. Wang, X. Ge, Electroanalysis, 24 (2012) 911-916.
[30] J. Zhang, K. Sasaki, E. Sutter, R.R. Adzic, Science, 315 (2007) 220-222.
[31] J. Greeley, J.K. Norskov, Surf. Sci. , 601 (2007) 1590-1598.
[32] J. Greeley, T.F. Jaramillo, J. Bonde, I. Chorkendorff, J.K. Norskov, Nat. Mater. , 5 (2006) 909-913.
[33] L.D. Burke, A.P. O'Mullane, V.E. Lodge, M.B. Mooney, J. Solid State Electrochem. , 5 (2001) 319-327.
[34] J.M. Booth, S.K. Bhargava, A.M. Bond, A.P. O'Mullane, J. Phys. Chem. B, 110 (2006) 12419-12426.
[35] S. Zein El Abedin, F. Endres, Electrochim. Acta, 54 (2009) 5673-5677.
[36] A.R. Harris, A. Nafady, A.P. O'Mullane, A.M. Bond, Chem. Mater., 19 (2007) 5499-5509.
[37] L.-S. Jou, J.-K. Chang, T.-J. Twhang, I.W. Sun, J. Electrochem. Soc., 156 (2009) D193-D197.
[38] I. Najdovski, P.R. Selvakannan, A.P. O'Mullane, S.K. Bhargava, Chem. Eur. J., 17 (2011) 10058-10063.
[39] C. Milhano, D. Pletcher, J. Electroanal. Chem., 614 (2008) 24-30.
[40] I. Najdovski, P.R. Selvakannan, S.K. Bhargava, A.P. O'Mullane, Nanoscale, 4 (2012) 6298-6306.
[41] H. Ataee-Esfahani, L. Wang, Y. Nemoto, Y. Yamauchi, Chem. Mater., 22 (2010) 6310-6318.
[42] J. Wang, R.M. Asmussen, B. Adams, D.F. Thomas, A. Chen, Chem. Mater., 21 (2009) 1716-1724.
[43] J.B. Xu, T.S. Zhao, S.Y. Shen, Y.S. Li, Int. J. Hydrogen Energy, 35 (2010) 6490-6500.
[44] S.-M. Hwang, J.E. Bonevich, J.J. Kim, T.P. Moffat, J. Electrochem. Soc., 158 (2011) B1019-B1028.
[45] J. Wang, G.M. Swain, J. Electrochem. Soc., 150 (2003) E24-E32.
[46] K.A. Homan, J. Chen, A. Schiano, M. Mohamed, K.A. Willets, S. Murugesan, K.J. Stevenson, S. Emelianov, Adv. Funct. Mater., 21 (2011) 1673-1680.

[47] B.J. Plowman, A.P. O'Mullane, P.R. Selvakannan, S.K. Bhargava, Chem. Commun., 46 (2010) 9182-9184.

List of figures

Figure 1: CVs recorded at 10 mV s^{-1} on a GC electrode in a 0.1 M HCl solution containing (a) 2.5 mM K_2PtCl_4, (b) 2.5 mM $HAuCl_4$ and (c) equimolar (2.5 mM) $HAuCl_4$ and K_2PtCl_4.

Figure 2: SEM images of (a) sample S1 and (b) S2. Scale bar is 2 μm in each case.

Figure 3: SEM images of (a1, a2) sample S5, (b1, b2) sample S4 and (c1, c2) sample S3. Scale bar is 2 μm in images (a1), (b1) and (c1) and 500 nm in images (a2), (b2) and (c2).

Figure 4: High magnification SEM images of samples (a) S4 and (b) S5. Scale bar is 200 nm in each case.

Figure 5: CVs recorded at 50 mV s^{-1} in 1 M H_2SO_4 at (a) samples S3, S4 and S5 and (b) samples S1 and S4.

Figure 6: XRD patterns for samples S3, S4 and S5. The corresponding peak positions for polycrystalline Pt (dashed line) and Au (dotted line) are provided referenced from JCPDS 04-0802 and JCPDS 04-0784 respectively.

Figure 7: (a) Linear sweep voltammograms recorded at 10 mV s^{-1} in 1 M H_2SO_4 at Pt (S1) and AuPt (S3 - S5) and (b) CVs recorded at 20 mV s^{-1} in 1 M H_2SO_4 and 1 M formic acid at Pt (S1), AuPt (S3 - S5) and commercial Pt/C.

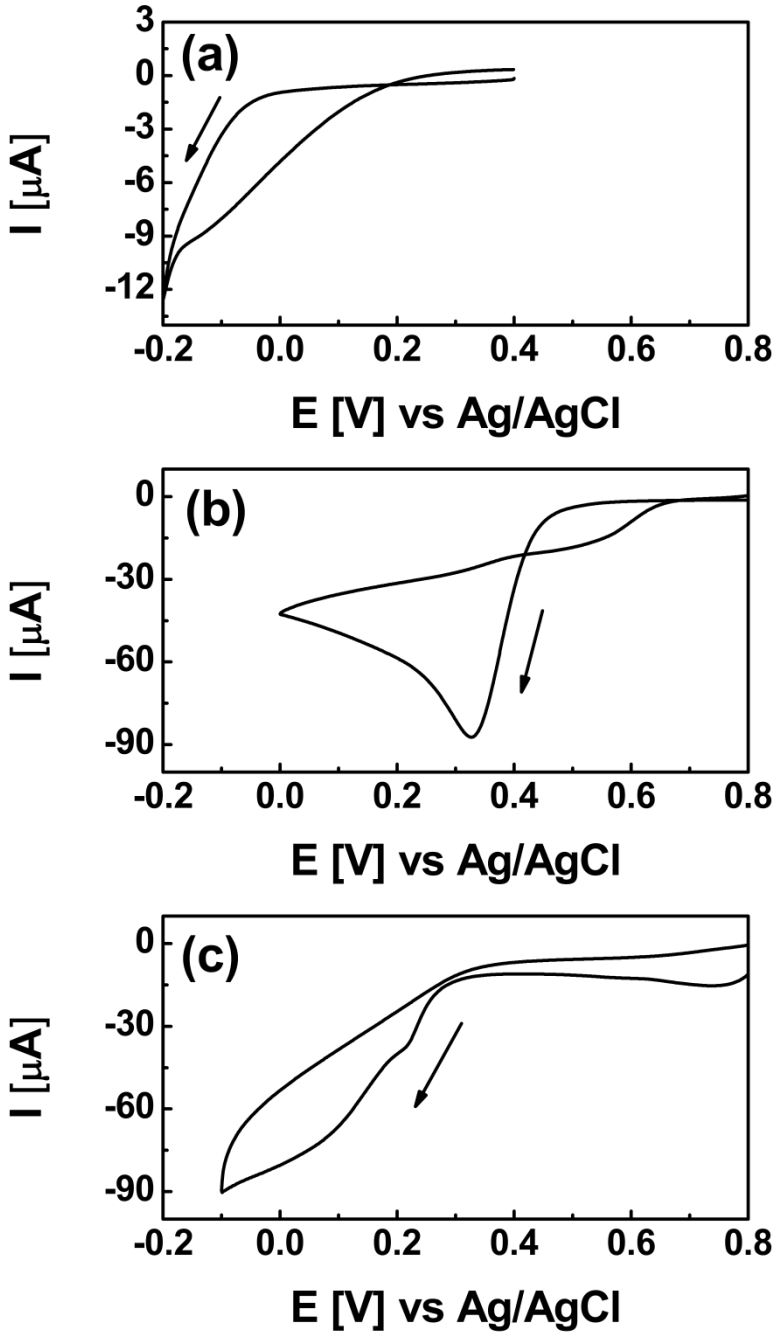
(a)
I [μA]
3
0
-3
-6
-9
-12
-0.2
0.0
0.2
0.4
0.6
0.8
E [V] vs Ag/AgCl
(b)
I [μA]
0
-30
-60
-90
-0.2
0.0
0.2
0.4
0.6
0.8
E [V] vs Ag/AgCl
(c)
I [μA]
0
-30
-60
-90
-0.2
0.0
0.2
0.4
0.6
0.8
E [V] vs Ag/AgCl

Figure 1:

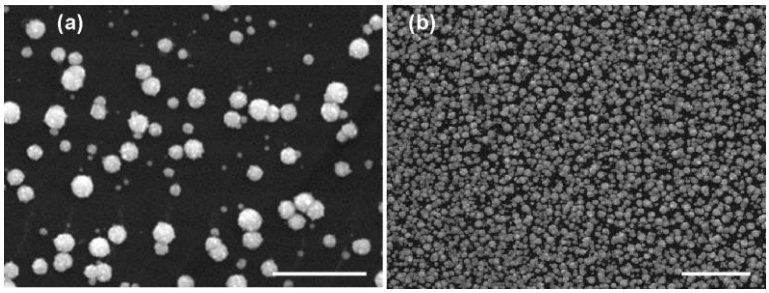

Figure 2:

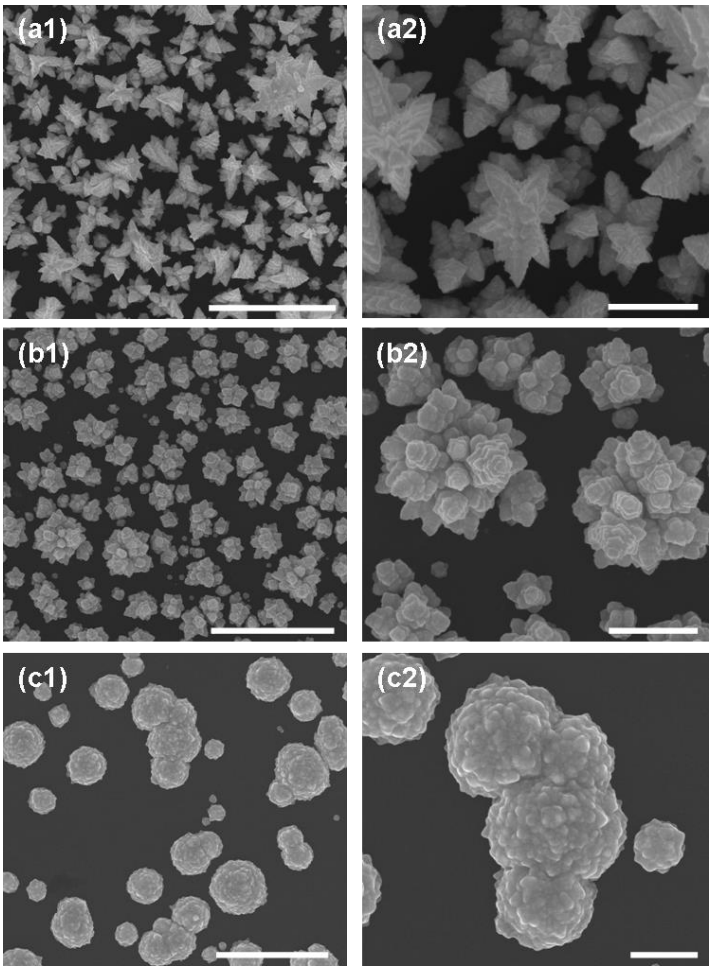

Figure 3:

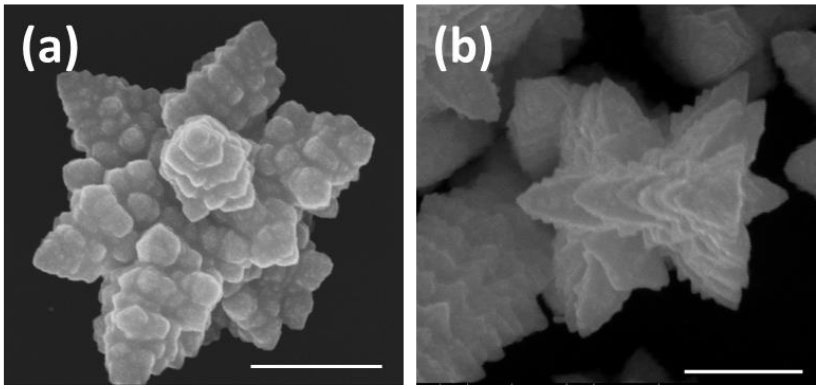

Figure 4:

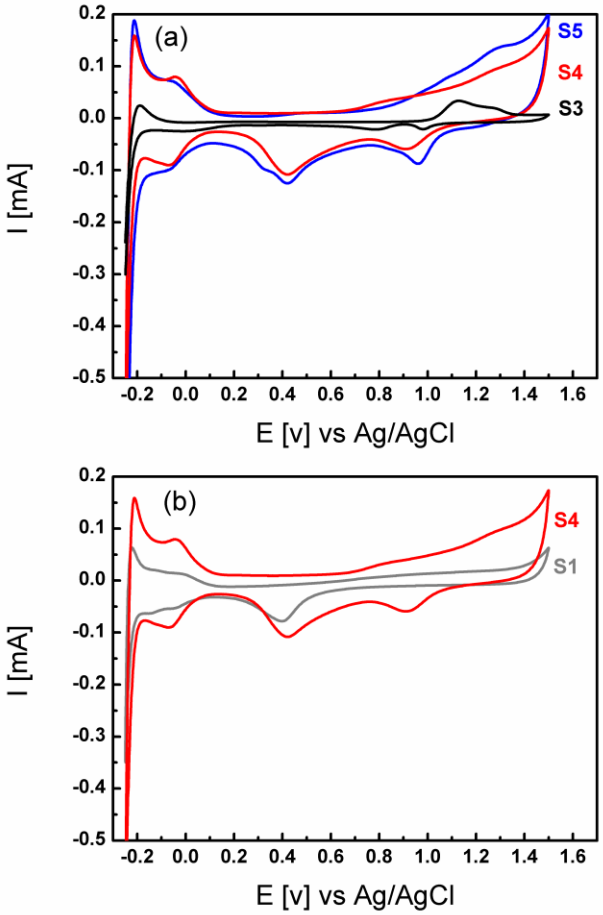

Figure 5:

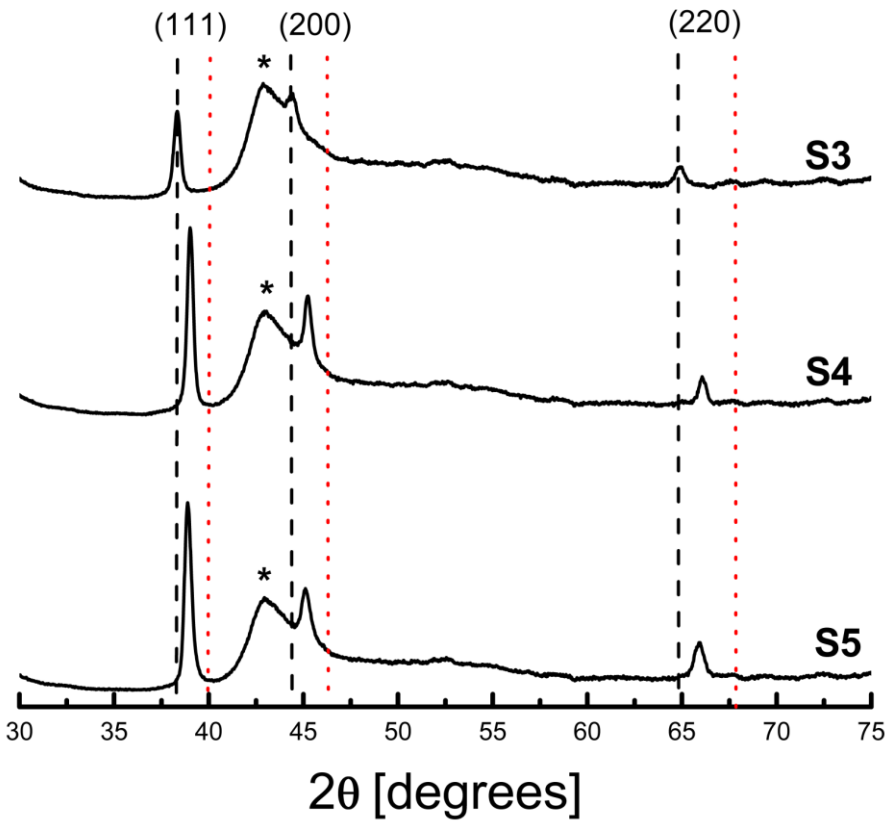

Figure 6:

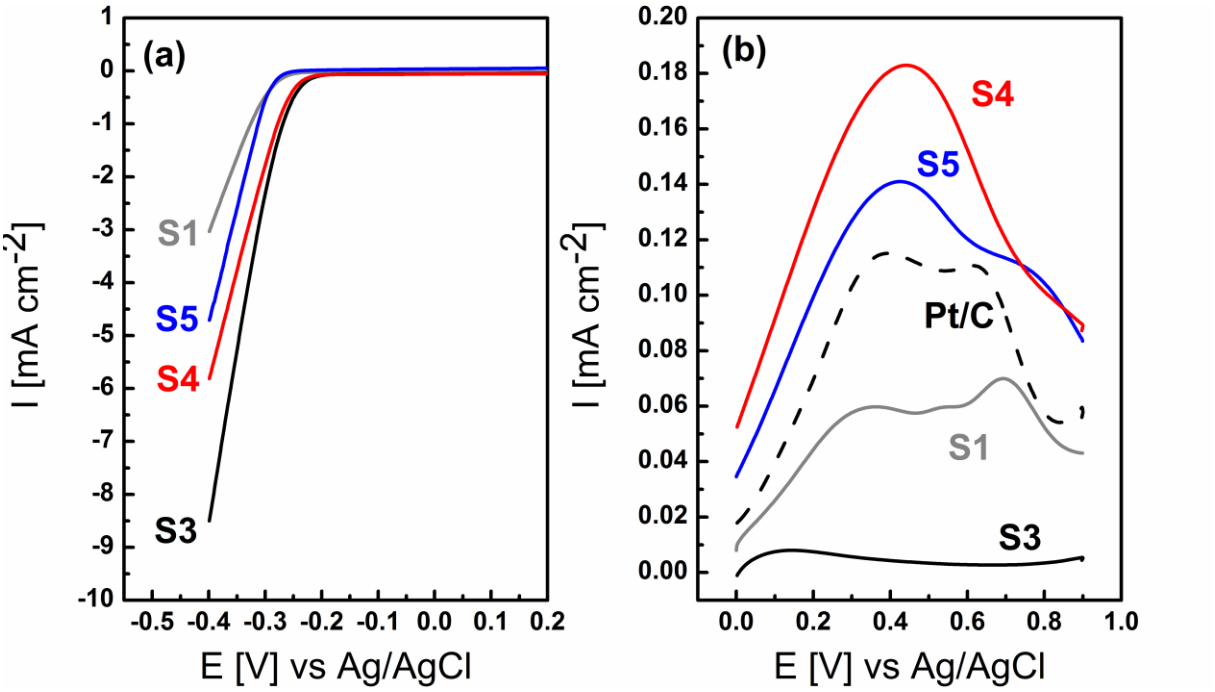
(a)
S1
S5
S4
S3
I [mA cm-2]
E [V] vs Ag/AgCl
(b)
S4
S5
Pt/C
S1
S3
I [mA cm-2]
E [V] vs Ag/AgCl

Figure 7: